PAPER

Check for updates

Fe-doped $H_3PMo_{12}O_{40}$ immobilized on covalent organic frameworks (Fe/PMA@COFs): a heterogeneous catalyst for the epoxidation of cyclooctene with H_2O_2

Dandan Yu,†[ab] Wenxiu Gao,†*[a] Shuyu Xing,[ab] Lili Lian,[a] Hao Zhang,[a] Xiyue Wang[a] and Dawei lou ⓘD *[a]

Covalent organic frameworks (COFs) have arisen as one kind of devisable porous organic polymer that has attracted immense attention in catalytic applications. In this work, we prepared cost-effective imine-based COFs (COF-300, COF-LZU1 and CIN-1) *via* a reaction kettle operated in place of a traditional sealed Pyrex tube. Then, phosphomolybdic acid (PMA) and iron ions were immobilized on the COF supports by impregnation; the resulting frameworks were denoted as Fe/PMA@COFs (Fe/PMA@COF-LZU1, Fe/PMA@CIN-1 and Fe/PMA@COF-300). A series of characterization results demonstrated that the PMA and iron ions were uniformly dispersed on the surface/cavities of the COFs. The catalytic properties of the obtained Fe/PMA@COFs were investigated in the epoxidation of cyclooctene with H_2O_2 as the oxidant. The experimental results show that the Fe/PMA@CIN-1 composite can act as an efficient heterogeneous catalyst for the epoxidation of cyclooctene. The intramolecular charge transfer between the COFs and the dual sites (PMA and Fe ions), the spatial structure and the nitrogen content of the COFs played critical roles in dispersing and stabilizing the active species, which are closely connected with the activity and stability of the catalysts. A novel efficient heterogeneous catalyst for the epoxidation of olefins *via* a simple and cost-effective process is provided, and this experiment demonstrates the notable application prospects of the covalent organic skeleton as a catalyst support.

Introduction

Covalent organic frameworks (COFs) are a class of crystalline organic porous materials that are constructed from light elements and linked by covalent bonds to create predesigned skeletons and nanopores.[1,2] By means of the organic functional group of the framework, a multitude of active sites are introduced into the porous network to develop COFs with diverse applications, such as gas storage and separation,[3–6] energy conversion,[7] optoelectronics,[8–10] and catalysis.[11–14] According to research, imine-based COFs are highly stable in water and common organic solvents; moreover, coordination chemistry demonstrates that imine-type ligands are versatile in incorporating a variety of metal ions.[15,16] Several kinds of imine-based COFs have been used as excellent candidates for catalytic applications.[12,15,17,18] Vaidhyanathan's group reported a nitrogen-rich and triazine-based COF (trzn-COF) loaded with

Pd^0 nanoparticles, named Pd-trzn-COF, as a good hydrolytically stable catalyst for multi-fold Heck and C–C coupling reactions.[17] An sp^2-rich non-polar phenyl framework and Schiff linkages serve as a polar matrix mimicking the environment typically present in homogeneous molecular catalysts.[18] Bhaumik and coworkers used a nitrogen-rich porous covalent imine network (CIN-1) material as an efficient catalytic support for C–C coupling reactions.[19] The stability of the catalyst is due to the intimate contact between the nitrogen-rich organic support and Pd nanoparticles.

The epoxidation of olefins is an important chemical industrial process. The preparation of more efficient heterogeneous catalysts for the aerobic epoxidation of olefins by an environmentally benign route has attracted considerable study interest in recent years. On the one hand, the seldomly employed oxygen oxidant hydrogen peroxide (H_2O_2) is the most popular environment-friendly reagent. Different kinds of heterogeneous catalysts have been widely investigated. Polyoxometalates (POMs) are one class of efficient epoxidation catalysts of olefins.[12,20,21] Noritaka Mizuno and his research group found that peroxotungstate immobilized on dihydroimidazolium-based ionic liquid-modified SiO_2 is an efficient heterogeneous epoxidation catalyst of various olefins with H_2O_2.[22] On the other

[a]Department of Analytical Chemistry, Jilin Institute of Chemical Technology, 45 Chengde Street, Jilin 132022, P. R. China. E-mail: dwlou@hotmail.com

[b]Department of Physical Chemistry, Jilin University, 2699 Qianjin Street, Changchun 130012, P. R. China

† These authors contributed equally.

hand, numerous transition metal complexes of iron have been investigated as alkene epoxidation catalysts.[23–26] Costas and coworkers developed a series of Fe-pdp catalysts with chiral tetradentate ligands for the epoxidation of a wide range of olefins.[27] In this work, iron coordination complexes bearing tetradentate aminopyridine ligands are shown to constitute a privileged platform for epoxidation. Carboxylic acid can be envisioned as a valuable partner to modulate the structure of oxygen atom species in reactions where peroxides are used as oxidants.

Previously, Jia and his group prepared various POMs or transition metal complex-based heterogeneous catalysts for olefin epoxidation.[28–34] As a follow-up work, in this study, we prepared cost-effective imine-based COFs (COF-LZU1, CIN-1, and COF-300) using a reaction kettle. Then, phosphomolybdic acid (PMA) and iron ions were immobilized onto the COF supports by impregnation, and the resulting materials were denoted as Fe/PMA@COFs (Fe/PMA@COF-LZU1, Fe/PMA@CIN-1, and Fe/PMA@COF-300). The physicochemical properties of the Fe/PMA@COFs were determined by a comprehensive range of characterization techniques, such as Fourier-transform infrared (FT-IR) spectroscopy, X-ray powder diffraction (XRD), scanning electron microscopy (SEM), transmission electron microscopy (TEM), N_2 adsorption/desorption and X-ray photoelectron spectroscopy (XPS), and their catalytic performances were tested in the epoxidation of cyclooctene with H_2O_2 as oxidant. The experimental results show that the Fe/PMA@CIN-1 composite can act as an efficient heterogeneous catalyst for the epoxidation of cyclooctene. The intramolecular charge transfer between the COFs and the dual sites (Fe and PMA ions), as well as the spatial structure and nitrogen content of the COFs, played critical roles in dispersing and stabilizing the active species, which are closely connected with the activity and stability of the catalysts.

Experimental

Preparation of imine-based COFs

COF-LZU1, CIN-1, and COF-300 were prepared *via* a simple and cost-effective process, using a reaction kettle (Teflon-lined stainless-steel autoclave) operated in place of a traditional sealed Pyrex tube. The reaction monomers were transferred to the reaction kettle and crystallization occurred at a lower temperature (COF-LZU1, CIN-1, and COF-300: 120 °C, 168 °C and 120 °C, respectively). The other steps were performed according to procedures described in the literature.[15,19,34] Among them, the nitrogen content of COF-LZU1, CIN-1 and COF-300 was 14.2%, 45% and 9.14%, respectively (Fig. 1).

Preparation of Fe/PMA@COFs

Fe/PMA@COF complexes were prepared by the impregnation method. All the chemicals used for synthesis were of analytical grade and commercially available. Ultrapure water was used in all experiments. COFs (0.1 g) were dispersed in 20 mL of ultrapure water under ultrasonic irradiation for 1 h. Afterward, a certain concentration of $H_3PMo_{12}O_{40}$ aqueous solution was

added to the above solutions with stirring at 80 °C. After 12 h of stirring, a certain concentration of $Fe(NO_3)_3 \cdot 9H_2O$ solution was added to the reaction flask, and the mixture was stirred continuously to guarantee reaction for 24 h at 80 °C. The product was filtered off, washed with water and ethanol, and dried at 80 °C overnight under vacuum to afford the Fe/PMA@COFs.

Results and discussion

Characterization techniques

FT-IR spectra were recorded on an Interspec 200-X FTIR spectrometer in the range 3500–500 cm^{-1}. XRD patterns were collected using a Bruker D8 Advance X-ray powder diffractometer in reflectance Bragg–Brentano geometry employing Ni-filtered Cu Kα line-focused radiation at 1600 W (40 kV, 40 mA) power. N_2 adsorption/desorption isotherms were measured at liquid nitrogen temperature using a Micromeritics ASAP 2020 automated adsorption analyzer. All samples were degassed at 393 K for 12 h before measurements. The surface areas were calculated using the Brunauer–Emmett–Teller (BET) method using the adsorption data in the relative pressure range of 0.05–0.2. Total pore volumes were derived at the relative pressure of $P/P_0 = 0.99$, assuming full surface saturation with nitrogen. Pore size distributions were calculated from the N_2 adsorption isotherms by non-linear density functional theory methods. The field-emission SEM images were obtained on an FEI Nova Nano SEM 450. TEM and energy-dispersive X-ray spectrometry (EDS) were carried out using a JEM-2100F electron microscope. XPS measurements were performed on a Thermo ESCALAB 250 system with a Mg Kα source (1253.6 eV).

Material characterization

Fig. 2 shows the FT-IR spectra of the PMA, COFs, and Fe/PMA@COFs. The characteristic peaks of the COFs in the whole region presented good agreement with the literature-reported results.[15,19,34] The existence of a strong C=N stretching vibration at around 1619 cm^{-1} is indicative of the formation of imine bonds during reaction kettle operation. This result confirms that the COFs (COF-LZU1, CIN-1 and COF-300) were successfully synthesized by using the reaction kettle method. Comparing the spectra of the Fe/PMA@COFs and COFs, the COF was well conserved after loading the PMA and Fe ions. The apparent red shift of the C=N peak indicated the coordination of Fe ions to imine N atoms in the framework.[35] The characteristic absorption peak of P–O_a at 1064 cm^{-1} in PMA shifted to around 1059 cm^{-1} after immobilization, indicating the chemical interaction between PMA and the COFs.[12] The characteristic peaks of Mo–O_b at 968 cm^{-1}, Mo–O_b–Mo at 870 cm^{-1}, and Mo–O_c–Mo at 798 cm^{-1} partially overlapped with the absorption peaks of the COFs.

Fig. 3 displays the XRD patterns of PMA, $Fe(NO_3)_3$, COFs and Fe/PMA@COFs. The main characteristic diffraction peaks of COF-LZU1, CIN-1 and COF-300 were preserved, indicating that doping of PMA caused no destruction of the structure of the support. The characteristic diffraction peaks of PMA and
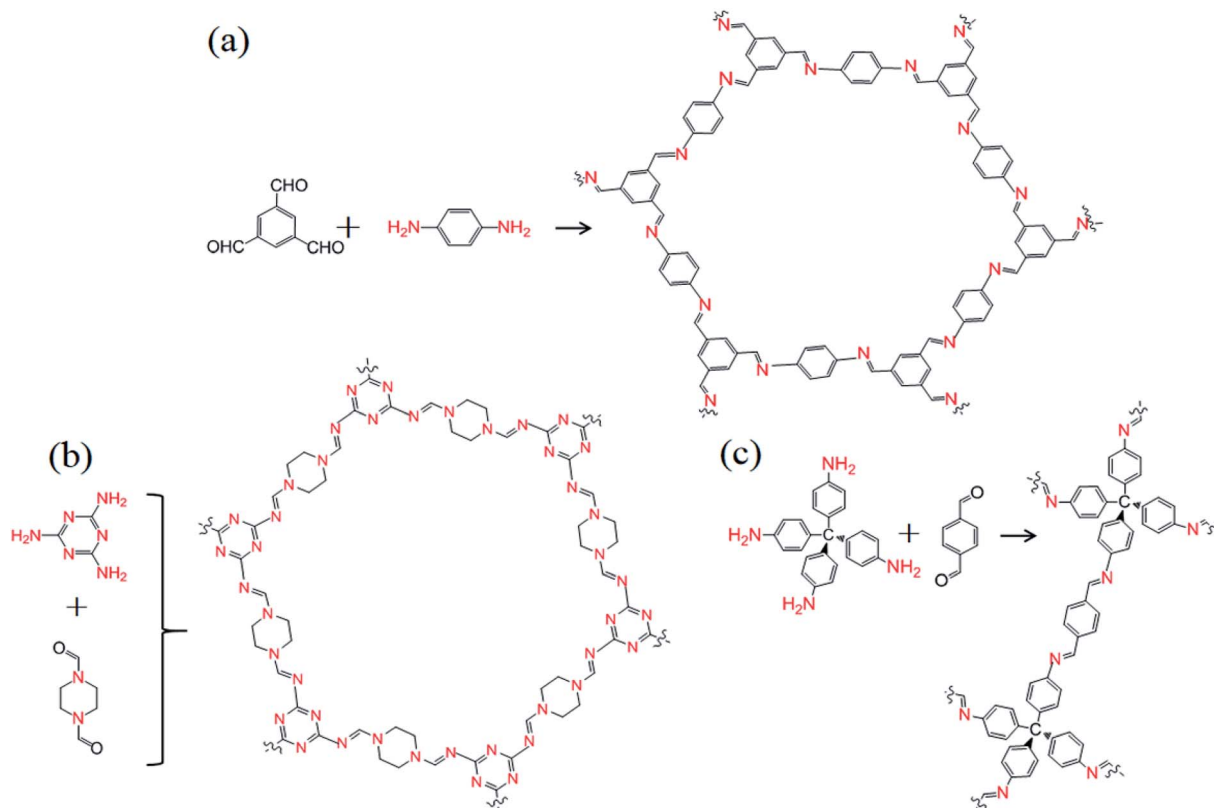
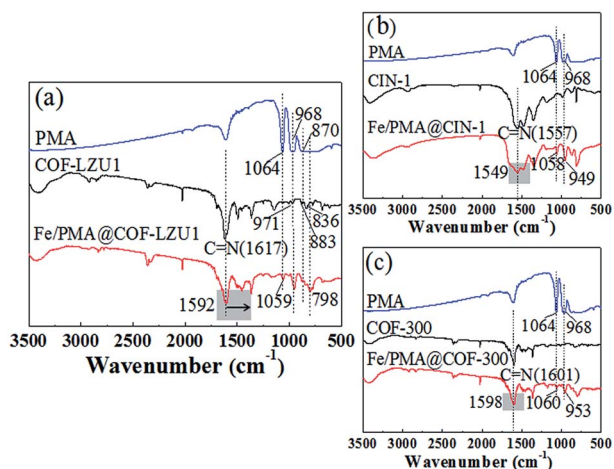Fig. 1 Construction of (a) COF-LZU1, (b) CIN-1, and (c) COF-300.
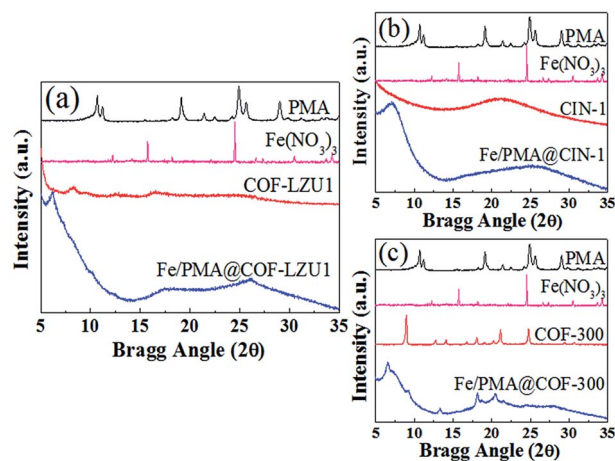

Fig. 2 FT-IR spectra of PMA, COFs and Fe/PMA@COFs.

Fig. 3 XRD spectra of PMA, COFs and Fe/PMA@COFs.

$Fe(NO_3)_3$ were absent in Fe/PMA@COFs, indicating that PMA is highly and molecularly dispersed within the surface and pores of the COF. With regard to the characteristic peaks of Fe/PMA@COFs, a decreased intensity, increased width, and significant shifts to high-angle regions were observed, suggesting that several cavities were filled with the introduced active substance.[36,37] The appearance of the new low-angle peaks in the Fe/PMA@COF-300 composites is similar to that observed in a previous report,[12] and this finding should be related to the distribution of PMA units and slight transformation of the COF-300 framework after introducing the PMA and Fe ions (Fig. 3c).[38–41]

Fig. 4 shows the SEM images of the COFs and Fe/PMA@COFs. The morphology of the COFs prepared via the reaction kettle is similar to literature findings (Fig. 4a, c and e).[15,19,34] The image of the Fe/PMA@COF-LZU1 composite shows a layered-sheet morphology with a size of around 300 nm (Fig. 4b).

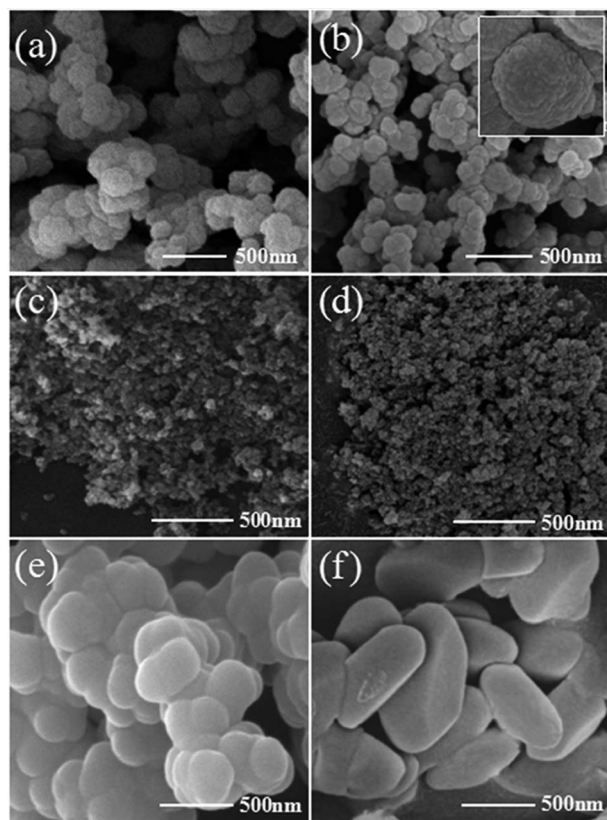The image of Fe/PMA@CIN-1 depicts spherical-like nanoparticles of size ca. 40–60 nm (Fig. 4d). A smaller packing

Fig. 4 SEM images of (a) COF-LZU1, (b) Fe/PMA@COF-LZU1, (c) CIN-1, (d) Fe/PMA@CIN-1, (e) COF-300, and (f) Fe/PMA@COF-300.

structure of particles usually features a larger surface area and better loading property. The Fe/PMA@COF-300 composite shows a similar morphology to the grain shape of rice, achieving better dispersion rather than agglomeration (Fig. 4f). From the morphology observed in the SEM images, we can preliminarily determine that the size of the COFs synthesized by the reactor was uniform and well dispersed, and no visible evidence of the accumulation of active species was found.

Fig. 5 displays the TEM images of Fe/PMA@COFs. Fe/PMA@COF-LZU1 can be observed to have an eclipsed layered-sheet arrangement (Fig. 5a and b). At first, several black spots were observed to be uniformly dispersed on the composite surface at a certain magnification in the TEM image. Lattice fringes can also be observed after extended irradiation, showing good agreement with the d spacing of the PMA crystal planes (424), (225), (521), (434) and (305) (Fig. 5c). Meanwhile, a similar phenomenon also occurred in Fe/PMA@COF-300. After an extended irradiation time, the crystal planes (512), (424), (306), (502), and (335) (PDF #46-0482 PMA) can be observed (Fig. 5i).

Notably, the morphology of COF-300 changed to a certain extent after introducing the PMA units and Fe ions, and a relatively rough surface appeared over the composite particles (Fig. 5g and h). These phenomena imply that the dopant not only dispersed on the outer surface of the carrier but also participated in the recrystallization process of COF-300, which is compatible with the carrier skeleton structure.[42–44]

Fig. 6a–c show the HAADF-STEM images of the Fe/PMA@COFs. As shown in the EDS mapping images, P and Mo originated from the PMA units, whereas Fe came from the loaded Fe ions (Fig. 6h, d and i). These images confirm that the PMA units and Fe ions were uniformly distributed over the whole composite. More Fe ions were also observed in Fe/PMA@CIN-1 compared with Fe/PMA@COF-LZU1 and Fe/PMA@COF-300 (Fig. 6b versus Fig. 6a and c). The Fe ions displayed a close relationship with the nitrogen content of the carriers. From this finding, we assumed that the Fe ions were loaded onto the COF by chemical reaction with C=N and physical adsorption.

Fig. 7 shows the nitrogen adsorption–desorption isotherms of the COFs and Fe/PMA@COFs. According to IUPAC classification, the COF-LZU1, CIN-1 and COF-300 samples exhibited type IV isotherms. A steep N_2 uptake at $P/P_0 < 0.01$ and $P/P_0 > 0.8$ characterized the micro- and macro-structure of the materials, and the increased nitrogen uptake above a partial pressure of 0.2 in the isotherm indicated the presence of mesopores. These characteristics show that the COFs prepared via the reaction kettle are hierarchically porous. Compared with the COFs, the BET surface areas and total pore volume of the Fe/PMA@COFs notably decreased (Table 1). This phenomenon indicates that certain amounts of PMA units and Fe ions were introduced not only on the surface of the COFs but also into the cavities. Moreover, significant changes in the pore size distributions suggest that the introduction of PMA units and Fe ions could block or destroy the pores of the COFs.

Fig. 8 provides the XPS measurements. Fig. 8a displays the N 1s spectra of the support CIN-1, PMA@CIN-1, and Fe/PMA@CIN-1. The binding energy (BE) of 399.2 eV is attributed to the nitrogen species in the imine groups of CIN-1. For PMA@CIN-1 and Fe/PMA@CIN-1, the peak of N 1s shifted to a lower position, with values of 398.9 and 397.2 eV, respectively. The N 1s peak moved toward to a lower level by 1 eV after doping Fe ions, further reflecting the presence of an interaction between Fe ions and the CIN-1 support. Combined with infrared characterization, it was found that the doping of PMA units and Fe ions is not merely a simple physical adsorption but also a coordination of chemical bonds. The Fe 2p spectrum was deconvoluted into one doublet Fe2p 1/2 at 723.1 eV and Fe2p 3/2 at 710.2 eV (Fig. 7b), which is attributed to the Fe^{3+} oxidation state. More importantly, compared with the pure iron oxide (BE of approximately 710.8 and 724.2 eV),[45–48] a minimal shift toward a lower BE of Fe^{3+} was observed in the catalyst composite, and this result may be due to the interaction between iron ions and the carrier.

Catalytic properties

The catalytic performances of the Fe/PMA@COFs composites were investigated in the epoxidation of cyclooctene with H_2O_2 as the oxidant. In order to ensure the accuracy of the experimental data, the results in Table 2 were repeated five times or more. Fe/PMA@COF-LZU1, Fe/PMA@CIN-1 and Fe/PMA@COF-300 respectively yielded 69% (s.d. = 2.4), 88% (s.d. = 1.3) and 62% (s.d. = 2.6) conversion values of cyclooctene with an
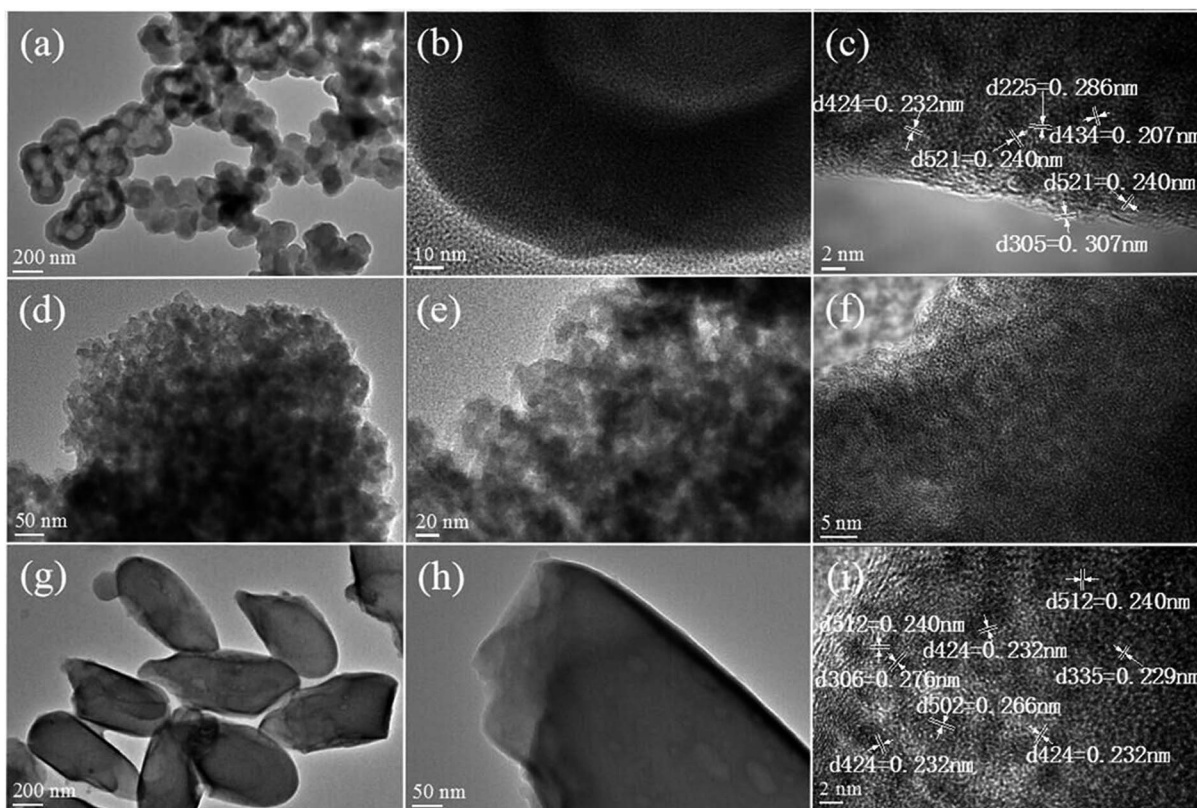
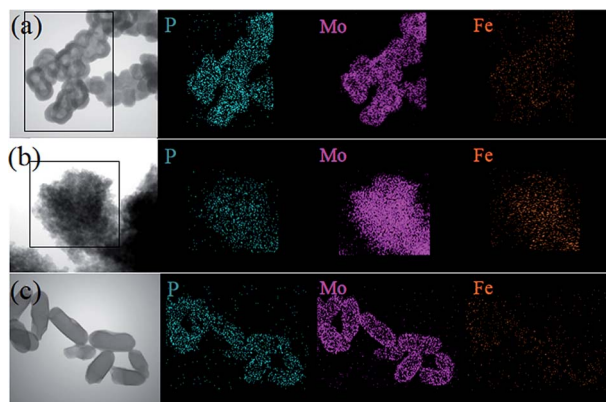**Fig. 5** TEM images of (a–c) Fe/PMA@COF-LZU1, (d–f) Fe/PMA@CIN-1, and (g–i) Fe/PMA@COF-300.

Fig. 6 EDS images of (a) PMA/Fe/COF-LZU1, (b) PMA/Fe/CIN-1, and (c) PMA/Fe/COF-300.

extremely high selectivity of epoxide (≥99%) after 9 h at 80 °C, and no detectable side products were observed under the test conditions (Table 2). PMA@COF-LZU1, PMA@CIN-1 and PMA@COF-300 respectively yielded 49% (s.d. = 2.3), 83% (s.d. = 1.4) and 52% (s.d. = 2.5) conversion values of cyclooctene. For comparison, the catalytic properties of PMA@COFs were also tested. PMA@COF composites showed 5–20% lower cyclooctene conversion values than the dual site catalyst Fe/PMA@COFs. Among these catalysts, Fe/PMA@CIN-1 is the most efficient. Moreover, the catalytic properties of Fe/PMA@CIN-1 were
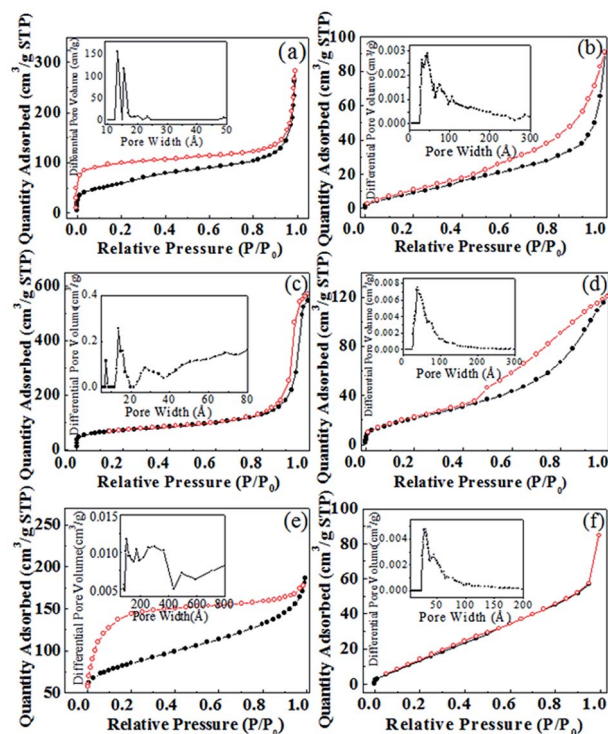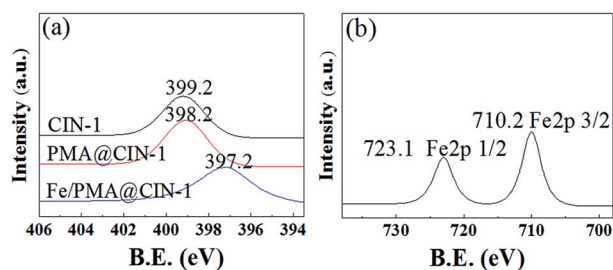

Fig. 7 N_2 adsorption–desorption isotherms and pore size distribution curve for (a) COF-LZU1, (b) Fe/PMA@COF-LZU1, (c) CIN-1, (d) Fe/PMA@CIN-1, (e) COF-300, and (f) Fe/PMA@COF-300.

Paper

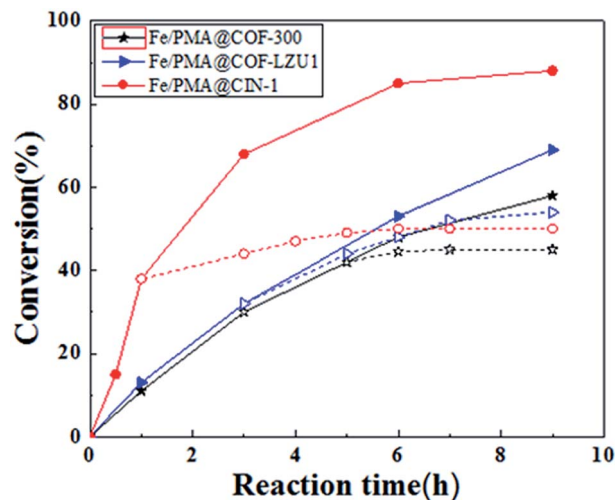**Table 1** Corresponding physicochemical properties of the as-prepared samples

Sample	S_{BET} [m^2 g^{-1}]	Pore size [Å]	Pore volume [cm^3 g^{-1}]
COF-LZU1	207	82	0.44
Fe/PMA@COF-LZU1	35	23	0.14
CIN-1	246	144	0.89
Fe/PMA@CIN-1	77	49	0.17
COF-300	284	36	0.25
Fe/PMA@COF-300	56	32	0.13

Fig. 8 X-ray photoelectron spectra of (a) N 1s and (b) Fe 2p.

Table 2 Reaction conditions: *cis*-cyclooctene 1.0 mmol, H$_2$O$_2$ 1.0 mmol, catalyst 10 mg, solvent (CH$_3$CN) 2 mL, 80 °C, 9 h. All selectivities for the epoxide are ≥99%

Substrate	Catalyst	Con. (%)	Selectivity (%)
	PMA@COF-LZU1	49	
	Fe/PMA@COF-LZU1	69	
	PMA@CIN-1	83	
	Fe/PMA@CIN-1	88	≥99
	PMA@COF-300	52	
	Fe/PMA@COF-300	62	
	Fe/PMA@CIN-1	58	≥99

further explored for the epoxidation of cyclododecene. It was found that this relatively bulky cyclododecene (with a kinetic diameter of around 8 Å) could also be converted to the corresponding epoxide over the dual site catalysts. These results suggest that PMA and Fe ions are distributed throughout the support, and most of them are easily accessible even for the bulky olefin. Combined with previous characterization, the results indicate that both PMA units and Fe ions play a crucial role in the catalytic process. The increased nitrogen content of the carriers is beneficial to introducing more Fe^{3+}, thus promoting the catalytic performance in the epoxidation reaction.

As shown in Fig. 9, the stability of the Fe/PMA@COF catalysts was investigated by leaching tests. In duplicate reactions, the solid catalyst was separated by hot filtration, and the filtrate was further stirred to study the continuing activity at the reaction temperature. When using the Fe/PMA@COFs, the epoxidation

Fig. 9 Reaction conditions: *cis*-cyclooctene: 1.0 mmol, H$_2$O$_2$: 1.0 mmol, catalyst: 10 mg, solvent (CH$_3$CN): 2 mL and 80 °C.

of cyclooctene was catalyzed with H$_2$O$_2$ as the oxidant. The catalyst was removed, and the conversion rate was measured. A small amount of cyclooctene conversion was observed within 2 h after separation of the solid catalyst Fe/PMA@COF-300 and Fe/PMA@CIN-1. After 2 h, no further increase in conversion rate was observed. This result may be due to the loss of the reactant *cis*-cyclooctene and a slight shedding of the active species during the separation operation, indicating the loss of a trace amount of active species to the reaction medium and the predominant heterogeneous catalysis. A relatively strong interaction is built between the dual-site units (Fe^{3+} and PMo$_{12}^{3-}$) and COF frameworks by intramolecular charge transfer, consistent with the previous characterization results. Therefore, it was proved that the stability of Fe/PMA@COF-300 and Fe/PMA@CIN-1 is high. On the contrary, the stability of Fe/PMA@LZUI is poor and the conversion rate continues to increase after separation of the solid catalyst. Combining the above catalytic data with the characterization results, it is clear that the configuration of the covalent organic skeleton is closely related to the stability of the catalysts. Fe/PMA@CIN-1 possesses an outstanding stability due to CIN-1 having a rich nitrogen content, small particle unit, and large surface area. Meanwhile, the 3-D structure of COF-300 can also assist in inhibiting active substance doping, which possibly explains why Fe/PMA@COF-300 showed a higher stability than Fe/PMA@COF-LZU1 (Fig. 9).

Conclusions

In this work, we prepared imine-based COFs (COF-300, COF-LZU1, and CIN-1) *via* a reaction kettle. PMA and iron ions were immobilized onto the COF supports to form Fe/PMA@COFs. A series of characterization methods verified that PMA and Fe ions were uniformly dispersed on the surface/cavities of the COFs. A relatively strong interaction was achieved between the dual-site units and COF frameworks. The

experimental results show that the Fe/PMA@CIN-1 composite can act as an efficient heterogeneous catalyst for the epoxidation of cyclooctene. The intramolecular charge transfer between COFs and the dual-site units (Fe and PMA) and the spatial configuration and nitrogen content of the COFs have played critical roles in dispersing and stabilizing the active species, which are closely connected with the activity and stability of the catalysts. This experiment demonstrates the notable application prospects of the covalent organic skeleton as a catalyst carrier.

Conflicts of interest

There are no conflicts to declare.

Acknowledgements

Notes and references

1 A. P. Côté, A. I. Benin, N. W. Ockwig, M. O'Keeffe, A. J. Matzger and O. M. Yaghi, *Science*, 2005, **310**, 1166.

2 F. J. Uribe-Romo, C. J. Doonan, H. Furukawa, K. Oisaki and O. M. Yaghi, *J. Am. Chem. Soc.*, 2011, **133**, 11478–11481.

3 H. Furukawa and O. M. Yaghi, *J. Am. Chem. Soc.*, 2009, **131**(25), 8875–8883.

4 Y. Pramudya and J. L. Mendoza-Cortes, *J. Am. Chem. Soc.*, 2016, **138**(46), 15204–15213.

5 J. L. Mendoza-Cortes, S. S. Han, H. Furukawa, O. M. Yaghi and W. A. Goddard, *J. Phys. Chem. A*, 2010, **114**, 10824–10833.

6 W. C. Song, X. K. Xu, Q. Chen, Z. Z. Zhuang and X. H. Bu, *Polym. Chem.*, 2013, **4**, 4690–4696.

7 H. B. Aiyappa, J. Thote, D. B. Shinde, R. Banerjee and S. Kurungot, *Chem. Mater.*, 2016, **28**(12), 4375–4379.

8 L. Chen, K. Furukawa, J. Gao, A. Nagai, T. Nakamura, Y. Dong and D. Jiang, *J. Am. Chem. Soc.*, 2014, **136**(28), 9806–9809.

9 S. Wan, F. Gándara, A. Asano, H. Furukawa, A. Saeki, S. K. Dey, L. Liao, M. W. Ambrogio, Y. Y. Botros, X. Duan, S. Seki, J. F. Stoddart and O. M. Yaghi, *Chem. Mater.*, 2011, **23**(18), 4094–4097.

10 Q. Xu, S. Tao, Q. Jiang and D. Jiang, *J. Am. Chem. Soc.*, 2018, **140**(24), 7429–7432.

11 D. B. Shinde, S. Kandambeth, P. Pachfule, R. R. Kumar and R. Banerjee, *Chem. Commun.*, 2014, **21**(2), 7944–7952.

12 W. Gao, X. Sun, H. Niu, X. Song, K. Li, H. Gao, W. Zhang, J. Yu and M. Jia, *Microporous Mesoporous Mater.*, 2015, **213**, 59–67.

13 H. Li, Q. Pan, Y. Ma, X. Guan, M. Xue, Q. Fang, Y. Yan, V. Valtchev and S. Qiu, *J. Am. Chem. Soc.*, 2016, **138**, 14783–14788.

14 P. Pachfule, A. Acharjya, J. Roeser, T. Langenhahn, M. Schwarze, R. Schomäcker, A. Thomas and J. Schmidt, *J. Am. Chem. Soc.*, 2018, **140**, 1423–1427.

15 S. Y. Ding, J. Gao, Q. Wang, Y. Zhang, W. G. Song, C. Y. Su and W. Wang, *J. Am. Chem. Soc.*, 2011, **133**, 19816–19822.

16 H. Zhang, X. Y. Wang, N. Li, J. H. Xia, Q. M. Meng, J. C. Ding and J. Lu, *RSC Adv.*, 2018, **8**, 34241.

17 D. Mullangi, S. Nandi, S. Shalini, S. Sreedhala, C. P. Vinod and R. Vaidhyanathan, *Sci. Rep.*, 2015, **5**(1), 1–10.

18 F. Wang, J. Mielby, F. H. Richter, G. H. Wang, G. Prieto, T. Kasama, C. Weidenthaler, H. J. Bongard, S. Kegnæs, A. Fürstner and F. Schüth, *Angew. Chem., Int. Ed.*, 2014, **126**, 8789–8792.

19 M. K. Bhunia, S. K. Das, P. Pachfule, R. Banerjee and A. Bhaumik, *Dalton Trans.*, 2012, **41**, 1304.

20 H. Kim, J. C. Jung, S. H. Yeom, K. Y. Lee and I. K. Song, *J. Mol. Catal. A: Chem.*, 2006, **248**, 21–25.

21 Y. Leng, J. Wu, P. Jiang and J. Wang, *Catal. Sci. Technol.*, 2014, **4**, 1293.

22 K. Yamaguchi, C. Yoshida, S. Uchida and N. Mizuno, *J. Am. Chem. Soc.*, 2005, **127**(2), 530–531.

23 D. Vidal, M. Costas and A. Lleó, *ACS Catal.*, 2018, **8**, 3667–3672.

24 W. Nam, H. J. Han, S. Y. Oh, Y. J. Lee, M. H. Choi, S. Y. Han, C. Kim, S. K. Woo and W. Shin, *J. Am. Chem. Soc.*, 2000, **122**, 8677–8684.

25 F. Yan, J. W. Munos, P. H. Liu and H. W. Liu, *Biochemistry*, 2006, **45**, 11473–11481.

26 S. Bhattacharjee, T. J. Dines and J. A. Anderson, *J. Phys. Chem. C*, 2008, **112**, 14124–14130.

27 O. Cussó, J. Serrano-Plana and M. Costas, *ACS Catal.*, 2017, **7**, 5046–5053.

28 J. Du, J. Yu, J. Tang, J. Wang, W. Zhang, W. R. Thiel and M. Jia, *Eur. J. Inorg. Chem.*, 2011, 2361–2365.

29 H. Gao, J. Yu, J. Du, H. Niu, J. Wang, X. Song, W. Zhang and M. Jia, *J. Cluster Sci.*, 2014, **25**, 1263–1272.

30 J. Wang, Y. Zou, Y. Sun, M. Hemgesberg, D. Schaffner, H. Gao, X. Song, W. Zhang, M. Jia and W. R. Thiel, *Chin. J. Catal.*, 2014, 35532–35539.

31 K. Li, J. Wang, Y. Zou, X. Song, H. Gao, W. Zhu, W. Zhang, J. Yu and M. Jia, *Appl. Catal., A*, 2014, **482**, 84–91.

32 X. Song, W. Zhu, K. Li, J. Wang, H. Niu, H. Gao, W. Gao, W. Zhang, J. Yu and M. Jia, *Catal. Today*, 2015, **259**, 59–65.

33 X. Song, W. Zhu, Y. Yan, H. Gao, W. Gao, W. Zhang and M. Jia, *J. Mol. Catal. A: Chem.*, 2016, **413**, 32–39.

34 F. J. Uribe-Romo, J. R. Hunt, H. Furukawa, C. Klöck, M. O'Keeffe and O. M. Yaghi, *J. Am. Chem. Soc.*, 2009, **131**, 4570–4571.

35 M. K. Bhunia, S. K. Das, P. Pachfule, R. Banerjee and A. Bhaumik, *Dalton Trans.*, 2012, **41**, 1304.

36 Z. Karimi, A. R. Mahjoub and F. Davari Aghdam, *Inorg. Chim. Acta*, 2009, **362**, 3725–3730.

37 Z. Karimi, A. R. Mahjoub and S. M. Harati, *Inorg. Chim. Acta*, 2011, **376**, 1–9.

38 W. Łuzny and M. Hasik, *Solid State Commun.*, 1996, **99**, 685–689.

39 E. S. Pomarzańska, M. Hasik, W. Turek and A. Proń, *J. Mol. Catal. A: Chem.*, 1996, **114**, 267–275.

40 S. Bureekaew, H. Sato, R. Matsuda, Y. Kubota, R. Hirose, J. Kim, K. Kato, M. Takata and S. Kitagawa, *Angew. Chem., Int. Ed.*, 2010, **49**, 7660–7664.

41 T. K. Maji, R. Matsuda and S. Kitagawa, *Nat. Mater.*, 2007, **6**, 142–148.

42 X. Feng, X. S. Ding and D. L. Jiang, *Chem. Soc. Rev.*, 2012, **41**, 6010–6022.

43 S. Wan, F. Gándara, A. Asano, H. Furukawa, A. Saeki, S. K. Dey, L. Liao, M. W. Ambrogio, Y. Y. Botros, X. F. Duan, S. Seki, J. F. Stoddart and O. M. Yaghi, *Chem. Mater.*, 2011, **23**, 4094–4097.

44 J. Li, X. D. Yang, C. Y. Bai, Y. Tian, B. Li, S. Zhang, X. Y. Yang, S. D. Ding, C. Q. Xia, X. Y. Tan, L. J. Ma and S. J. Li, *J. Colloid Interface Sci.*, 2015, **437**, 211–218.

45 X. Liang, R. Yang, G. Li and C. Hu, *Microporous Mesoporous Mater.*, 2013, **182**, 62–72.

46 S. Yang, G. Liang, A. Gu and H. Mao, *Appl. Surf. Sci.*, 2013, **285**, 721–726.

47 N. S. McIntyre and D. G. Zetaruk, *Anal. Chem.*, 1977, **49**, 1521–1529.

48 L. Sun, Y. Y. Cai, T. Ji and G. Y. Zhang, *RSC Adv.*, 2018, **8**, 35337.